Dynamics of Nanoparticle Self-Assembly into Superhydrophobic Liquid Marbles during Water Condensation

Konrad Rykaczewski,[†,*] Jeff Chinn,[‡] Marlon L. Walker,[†] John Henry J. Scott,[†] Amy Chinn,[‡] and Wanda Jones[‡]

[†]Material Measurement Laboratory, National Institute of Standards and Technology, Gaithersburg, Maryland 20899-8320, United States and, [‡]Integrated Surface Technologies, Inc., 1455 Adams Drive, Suite 1125, Menlo Park, California 94025, United States

ABSTRACT

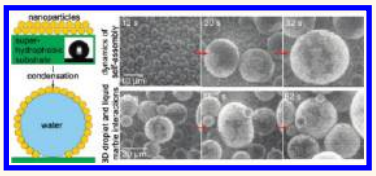

Nanoparticles adsorbed onto the surface of a drop can fully encapsulate the liquid, creating a robust and durable soft solid with superhydrophobic characteristics referred to as a liquid marble. Artificially created liquid marbles have been studied for about a decade but are already utilized in some hair and skin care products and have numerous other potential applications. These soft solids are usually formed in small quantity by depositing and rolling a drop of liquid on a layer of hydrophobic particles but can also be made in larger quantities in an industrial mixer. In this work, we demonstrate that microscale liquid marbles can also form through self-assembly during water condensation on a superhydrophobic surface covered with a loose layer of hydrophobic nanoparticles. Using *in situ* environmental scanning electron microscopy and optical microscopy, we study the dynamics of liquid marble formation and evaporation as well as their interaction with condensing water droplets. We demonstrate that the self-assembly of nanoparticle films into three-dimensional liquid marbles is driven by multiple coalescence events between partially covered droplets and is aided by surface flows causing rapid nanoparticle film redistribution. We also show that droplet and liquid marble coalescence can occur due to liquid-to-liquid contact or squeezing of the two objects into each other as a result of compressive forces from surrounding droplets and marbles. Irrelevant of the mechanism, coalescence of marbles and drops can cause their rapid movement across and rolling off the edge of the surface. We also demonstrate that the liquid marbles randomly moving across the surface can be captured and immobilized by hydrophilic surface patterns.

KEYWORDS: water condensation · ESEM · superhydrophobic surfaces · liquid marbles · self-assembly

Particles with similar wetting properties adsorbed onto a gas–liquid interface experience mutually attractive forces due to lateral capillary forces created by the deformation of the liquid surface.[1] As a result of this so-called "Cheerios effect",[1,2] floating breakfast cereal as well as nanoparticle dispersions tends to aggregate into films with properties similar to that of an elastic solid.[2,3] When formed on a drop, the particle film can fully encapsulate the liquid, creating a robust and durable[4,5] soft solid with superhydrophobic characteristics[6] referred to as a liquid marble.[5,7,8] When in contact with a solid surface, liquid marbles exhibit solid-like behavior with a nearly 180° contact angle and rolling rather than sliding motion.[9,10] These soft solids are common in nature, forming, for example, when rain falls on hydrophobic soil created by a wild fire.[11] Liquid marbles can also be created by insects.[12,13] For instance, aphids coat honeydew droplets in wax nanoparticles during defecation to prevent being entrapped and drowning in their own sugary excrement.[12,13] Artificially created liquid marbles have been studied only for about a decade[5,7,8] but are already utilized in some hair and skin care products.[14] Numerous other potential applications for liquid marbles such as liquid storage,[15,16] microreactors,[17] gas[18,19] and pollution[20] sensors, micropumps,[21] and even templates for spherical structures[22] have also been demonstrated. Macroscale liquid marbles are usually formed in small quantity by depositing and rolling a drop of liquid on a layer of hydrophobic particles,[7,8] but larger quantities of microscale liquid marbles can also be made in an industrial mixer.[16,23–25] In this work, we demonstrate that microscale liquid marbles can also form through self-assembly during water condensation on a superhydrophobic surface (SHS) covered with a loose layer of hydrophobic nanoparticles. Using *in situ* environmental scanning electron microscopy (ESEM)[26] and optical microscopy, we study the dynamics of liquid marble formation and evaporation as well as their interaction with condensing water droplets. We show that these processes involve a variety of unique dynamic three-dimensional phenomena resulting from a combination of solid-like and liquid-like behaviors. We also introduce a

* Address correspondence to konrad.rykaczewski@nist.gov.

Received for review August 24, 2011 and accepted October 27, 2011.

Published online October 28, 2011
10.1021/nn203268e

method for site-specific immobilization of randomly moving liquid marbles using hydrophilic grooves patterned onto the SHS.

RESULTS AND DISCUSSION

We study water condensation occurring on a multilayer Al_2O_3 nanoparticle film modified with a perfluorinated silane coating dispersed on naturally hydrophilic silicon, a hydrophobic silicon surface modified with a perfluorinated silane coating, and SHS consisting of Al_2O_3 nanoparticles encapsulated in a glass-like matrix and modified with a perfluorinated silane coating.[27] Following sufficient water condensation onto all of the surfaces, the nanoparticles migrate from the solid to the liquid surface and aggregate into floating rafts (see Figure 1). The nanoparticle patches thus formed pack sufficiently tightly to support condensation of secondary microdroplets (see Figure 1b–e and movie 1 in Supporting Information corresponding to Figure 1e). The nearly spherical shapes of the condensed secondary microdroplets demonstrate that the particle films are superhydrophobic and retain their wetting properties during condensation. It is important to note that most SHS are wet completely following sufficient condensation and only selected natural[28–30] and artificial[31–36] surfaces with properly designed surface chemistry and nanoscale and microscale topography[37,38] retain their superhydrophobic characteristics during condensation.[31,32,35,39,40] The particle films conform to the shape of the water interface, with nearly flat floating rafts forming on the hydrophilic silicon and liquid marbles forming on the SHS. The three-dimensional self-assembly process and secondary droplet condensation occur under partial vacuum conditions in the ESEM (see Figure 1b–d) as well as standard conditions for temperature and pressure (see Figure 1e). On the basis of the visual information presented, one could form a naïve hypothesis that the three-dimensional structures form when nanoparticles are picked up from below by condensing droplets in an inflating-balloon-type process. By studying the dynamics of the process, we reveal that the liquid marbles are formed in a far more complex manner.

The lack of visible nanoparticles on the water surface during the early stage of the condensation process suggests that, initially, individual droplets grow mostly on top of the multilayer nanoparticle film (see Figure 2a). In contrast, even with only monolayer nanoparticle coverage of the SHS, a hypothetical spherical drop with radius R growing directly on the surface would have clearly visible initial surface nanoparticle coverage of $\pi R^2/4\pi R^2$ or 25%. Furthermore, the initially high degree of droplet pinning decreases over time to a level typical for condensation occurring directly on a bare SHS.[39–41] The nonsymmetrical shapes of the droplets could be caused by insufficient packing of the loose nanoparticles to form a SHS[11,42,43] and some degree of

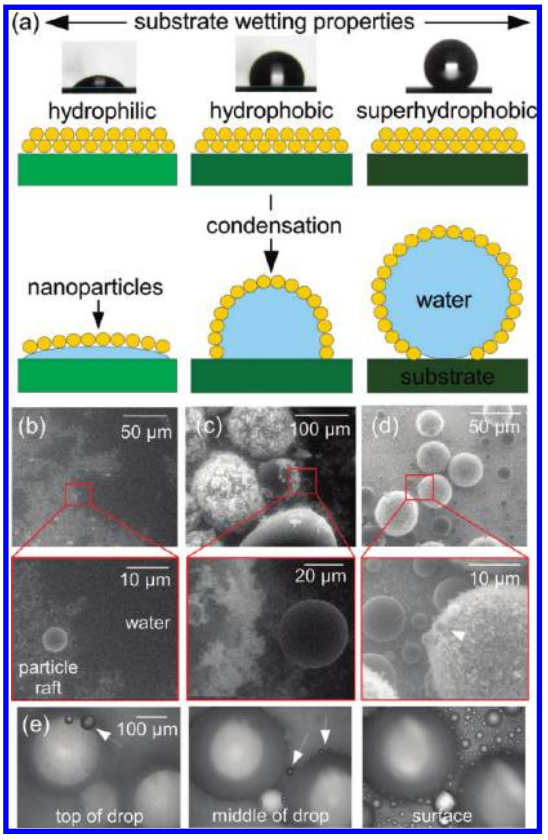

Figure 1. (a) Schematic of the dependence of the self-assembled nanoparticle film geometry on the wetting properties of the underlying substrate and optical images of water drops deposited on the substrates without the presence of nanoparticles. (b–d) ESEM images of nanoparticle films formed following water condensation onto (b) the hydrophilic silicon surface, (c) the hydrophobic silicon surface modified with perfluorinated silane, and (d) the superhydrophobic surface formed from Al_2O_3 nanoparticles encapsulated in a glass-like matrix and modified with a perfluorinated silane coating. (e) Optical images of liquid marbles formed on the nanoparticle-covered superhydrophobic surface as in (d) but under the standard conditions for temperature and pressure. The focus is adjusted to three vertical positions indicated in the images to reveal secondary droplet condensation on multiple locations on the self-assembled liquid marble. In all images, white arrows indicate position of secondary droplets.

capillary condensation.[44] Past initial nucleation, the drop nanoparticle surface coverage can increase *via* two mechanisms. In the first mechanism, the nanoparticles can migrate to the drop surface *via* liquid vapor meniscus as the drop expands over additional nanoparticles by direct vapor condensation. In the second mechanism, the nanoparticles can move from below to the side or the top of the drops during a coalescence event between two drops. In general, the dominating drop growth mechanism can be systematically determined by evaluating the average drop diameter, $\langle d \rangle$, as a function of time.[45–48] Typically $\langle d \rangle$ grows according to the power law $\langle d \rangle \sim t^{\alpha}$, where $\alpha = 1/3$ for individual droplet growth *via* direct vapor condensation irrelevant of surface properties and $\alpha = 1$ or $\alpha = 0$ for coalescence dominated growth on patterned hydrophobic[49–52] or

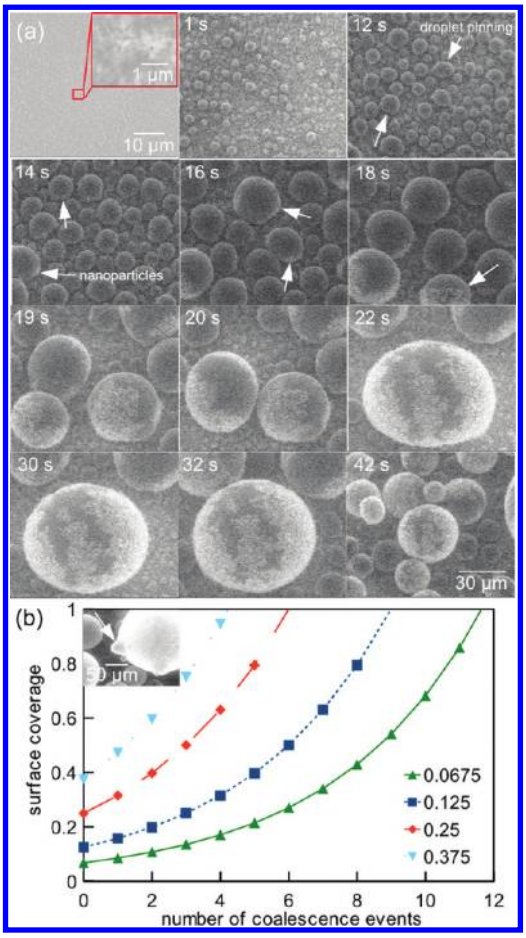

Figure 2. (a) Time sequence of ESEM images showing the dynamics of liquid marble self-assembly during condensation on a SHS and (b) surface coverage as a function of the number of coalescence events between two identical spherical drops with the same nanoparticle surface coverage. The inset in the left top corner shows an example of a bump on top of a liquid marble with saturated nanoparticle surface coverage formed after coalescence with a smaller liquid marble.

SHS, respectively.[31,53] Unfortunately, the ESEM experiments are performed in pressure-varying mode,[39,54] implying that the drops do not grow under steady state conditions, and fitting the growth rate law is not an appropriate method of determining the dominating drop growth mechanism (see further discussion in Supporting Information). However, drop growth *via* coalescence is likely the dominating growth mechanism because of the drastic decrease in the total number of drops from ~150 to ~20 during the 6 to 18 s time range in the process shown in Figure 2a (also see Figure 2 in Supporting Information). Furthermore, the decrease in the total drop number is accompanied by increase in $\langle d \rangle$ and emergence of visible nanoparticle coverage of the droplets. In the following 25 s, the droplet's nanoparticle surface coverage clearly increases with the number of coalescence events (see movie 2 in Supporting Information). This trend can be easily explained by evaluating the nanoparticle surface coverage as a function of the

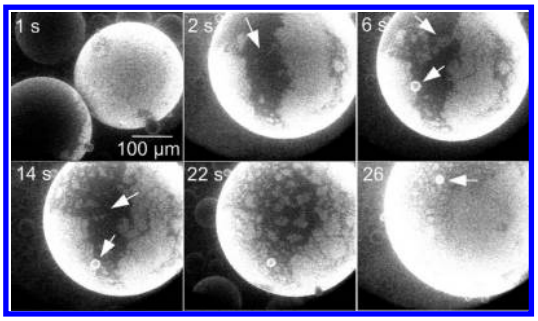

Figure 3. Time sequence of ESEM images showing surface movement of a nanoparticle film on top of a partially covered liquid marble formed after coalescence of a similarly sized liquid marble and water drop.

number of coalescence events between two identical spherical drops with common radius R_0 (corresponding to surface area $A_0 = 4\pi R_0^2$) and a common initial nanoparticle surface coverage C_0. The new drop resulting from the merging of the two parent drops will have a diameter of $R_1 = 1.26R_0$, surface area of $A_1 = 4\pi R_1^2 = 4\pi(1.58R_0^2)$, and a nanoparticle surface coverage of $2C_0(4\pi R_0^2)/(4\pi R_1^2)$ or $1.26C_0$. The surface coverage of the newly formed drop is higher than that of the individual parent drops because the total number of nanoparticles remains unchanged but total surface area decreases ($A_1/2A_0 = 0.79$) during the coalescence event. Figure 2b shows that, for this idealized case, a full nanoparticle surface coverage is reached within 12 coalescence events even for C_0 as low as 6.7%. Also, there is clear experimental evidence that excess nanoparticles can be added to a fully covered drop (*i.e.*, surface coverage greater than 1 is possible). In an extreme case shown in the inset in Figure 2b, coalescence of a small liquid marble with a larger fully covered marble results in creation of a bump consisting of stacked nanoparticles on the surface of the larger sphere. Even without being fully encapsulated in nanoparticles, the droplets begin to exhibit solid-like properties of liquid marbles. For example, 42 s into the condensation process the nearly fully covered droplets do not coalesce when coming in contact with other drops and stack on top of each other. It is interesting to note that a reverse mechanism has been observed in the literature. Namely, liquid marbles can be divided into separate marbles only a few times before losing their solid-like characteristics.[8,55] In this case, the total surface area of the newly formed marbles increases with each division, eventually diluting the particle surface coverage to the point that the marbles behave as liquid drops.

Droplet surface flows play an important role in the formation of liquid marbles through standard methods[14,56−60] as well as their self-assembly during water condensation. In the case of the standard methods for liquid marble formation, surface and internal flows arise due to the kinetic energy of droplet impact or rolling on hydrophobic powder. When a drop is deposited carefully onto a hydrophobic powder, liquid marble

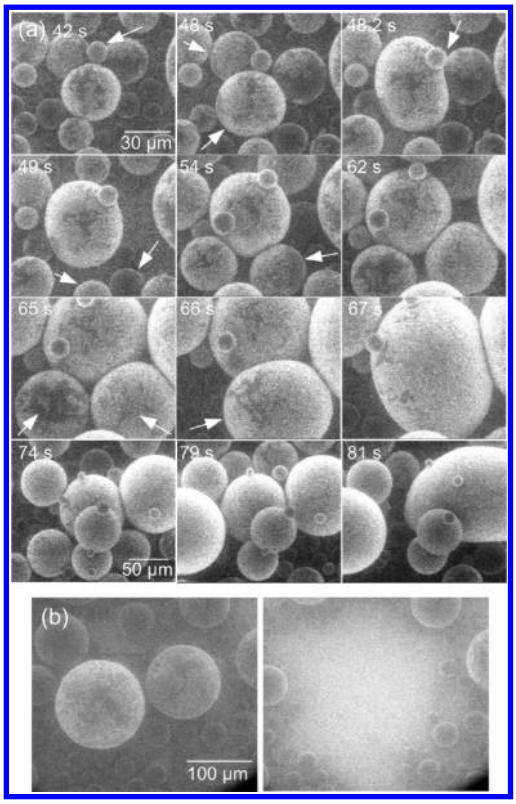

Figure 4. Time sequence of ESEM images showing (a) water condensation dynamics on a SHS in the presence of self-assembled liquid marbles. (b) Coalescence-triggered liquid marble movement.

formation is not observed[57] unless the drop is allowed to mostly evaporate.[11] In contrast, strong surface flows are observed in stationary drops and in partially formed liquid marbles during water condensation. For example, in the sequence of ESEM images shown in Figure 3, strong surface flows evidently contribute to the nanoparticle film reorganization after a coalescence event between partially and nearly fully covered drops. Interestingly, secondary droplets or small liquid marbles formed on the particle films are transported by the flow and reposition themselves on the surface of the primary drop along with the films (see Figure 3 and movie 3 in Supporting Information). Surface and internal flows during the condensation of microscale droplets can be caused by a coalescence event[61] or the thermocapillary Marangoni effect.[62] These strong surface flows allow for quick redistribution of the nanoparticle films on the surface of drops and accelerate the formation of the liquid marbles. Furthermore, exposure of a liquid surface due to film reorganization could also trigger a coalescence event.

The presence of self-assembled liquid marbles dramatically alters the nature of the condensation process on the SHS. The combination of their mechanical rigidity and the superhydrophobic nature of their self-assembled surfaces reduces the number of coalescence events. The presence of numerous liquid marbles

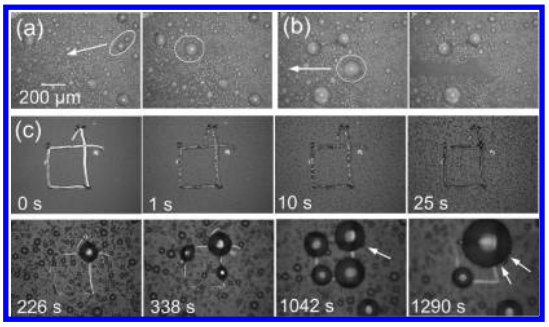

Figure 5. Time sequences of optical images showing (a) short-range and (b) long-range movement of liquid marbles after coalescence, (c) preferential water condensation and selective immobilization of liquid marbles on scratched hydrophilic grooves. White arrows in (a,b) indicate direction of the drop translation and in (c) indicate position of secondary droplets.

also significantly increases the surface area available for nucleation of new water droplets. The cumulative result of these effects is a highly dynamic and fully three-dimensional condensation process in which solid-like interactions become as important as liquid-like interactions. Multiple levels of drop-on-marble, marble-on-marble, and marble-on-drop stacking shown in Figure 4a highlight the three-dimensional nature of the process.

Typically, the merging of two artificially made liquid marbles is difficult[10] and can be achieved only through collision of marbles with high velocity[63] or through a strong external stimulus such as substrate vibration[64] or magnetic field.[17,63,65,66] In contrast, self-assembled liquid marbles readily coalesce with other liquid marbles and drops. Careful examination of the sequential ESEM images shown in Figure 4a reveals that liquid marbles can merge with other liquid marbles or drops *via* two different mechanisms. The first mechanism is typical for condensation and occurs due to liquid-to-liquid contact on the surface of two drops or partially covered liquid marbles. This type of event occurs, for example, between the two central liquid marbles 48 s into the condensation process (Figure 4a and movie 4 in Supporting Information). In the second mechanism, coalescence is induced by the pushing of two liquid marbles or a liquid marble and a droplet into each other by surrounding droplets and marbles. Coalescence occurs only after significant force is exerted on the two objects and is accompanied by a significant degree of deformation prior to coalescence. The second coalescence mechanism is evident from images of deformed liquid marbles being "squeezed into each other" at 48.2, 66, and 79 s into the condensation process, as depicted in Figure 4. Regardless of how the coalescence event was triggered, it can cause rapid motion and possible departure of the newly formed marbles and droplets from the surface (see Figure 4b).[31,67]

To study the later stages of the liquid marble behavior, we optically image water condensation onto the SHS with multilayer nanoparticle film occurring under

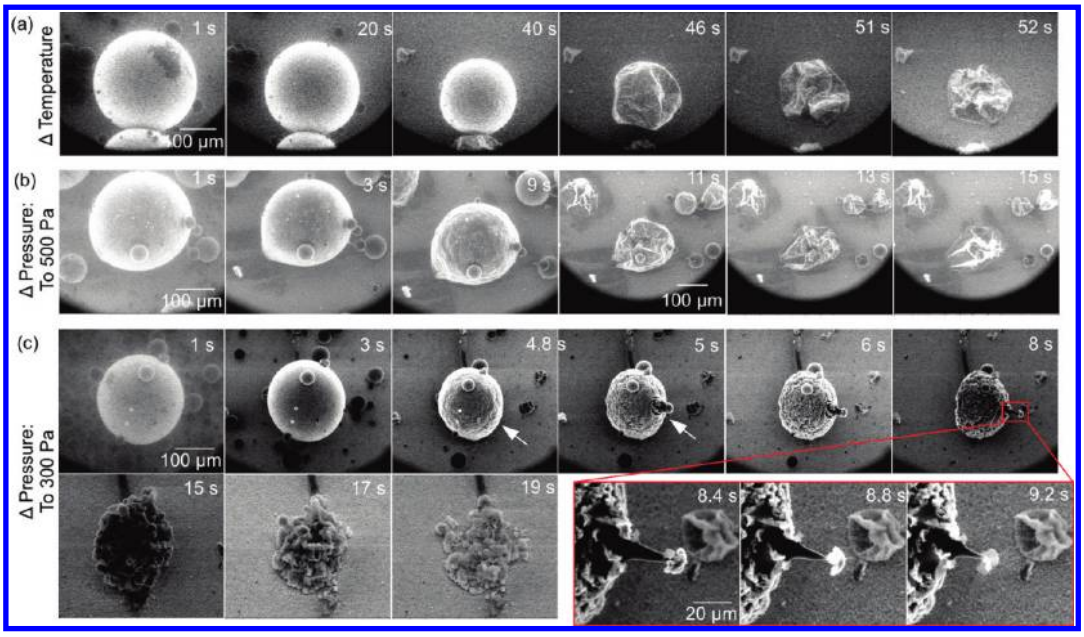

Figure 6. Time sequence of ESEM images showing evaporation of liquid marbles due to (a) a temperature increase at nearly constant pressure, (b) a pressure decrease to about 500 Pa, and (c) a pressure decrease to about 300 Pa.

standard conditions for temperature and pressure (see Methods section for details). Liquid marbles form and are present on the surface during the whole duration of the 40 min condensation experiment (see Figure 1e for example of observed liquid marble with secondary drops and movie 1). As in the ESEM experiments, coalescence of larger (diameters above ≈20 μm) liquid marbles and drops causes the newly formed object to move across the surface. The distance the newly formed marbles or drops travel after coalescence varies from tens of micrometers to several millimeters (see Figure 5a,b and movie 5). We also observe that the moving marbles and drops do roll off the edge of the surface. Consequentially, as in the case of water condensation on a bare SHS,[35,53] we do not observe liquid marbles and droplets with diameters larger than 300 to 400 μm. During the experiment, we noticed that spontaneously moving liquid marbles can be immobilized on the SHS by introducing local hydrophilic defects. We demonstrate that such site-specific immobilization of liquid marbles is possible by using metal tweezers to scratch out a square pattern onto the SHS prior to initiation of water condensation. As shown in Figure 5c, water preferentially condenses[49,68] and fills the hydrophilic scratched grooves within 25 s of lowering the substrate temperature. Throughout the rest of the experiments, liquid marbles passing through the filled grooves are stopped. The immobilized liquid marbles grow by coalescing with neighboring or moving marbles and drops (see movie 6 in Supporting Information). The presence of numerous secondary droplets on the surface of the immobilized liquid marbles shown in Figure 5c demonstrates that the immobilized liquid marbles retain superhydrophobic characteristics over extended periods of time.

Having explored the dynamics the early and the late stages of formation, we turn our attention to the dynamics of liquid marble and water droplet evaporation caused by an increase in the substrate temperature or a decrease in the chamber pressure. In agreement with previous reports,[4,22,69−73] increasing the substrate temperature results in the evaporation of surrounding water droplets as well as liquid marble shrinking, crumbling, and eventual collapse (see Figure 6a and movie 7 in Supporting Information). Similar but significantly faster behavior is observed when the liquid marble and surrounding water droplet evaporation is caused by a decrease in the surrounding water vapor pressure to a value slightly below the pressure corresponding to the triple point of water (a decrease from 750 Pa to about 500 Pa—see Figure 6b and movie 8 in Supporting Information). The liquid marbles likely evaporate faster in response to the surrounding pressure decrease than during the substrate temperature increase because change in pressure affects the whole surface area of the marble while substrate−marble heat transfer occurs through a small interfacial area. Regardless of the cause of evaporation, surrounding water droplet evaporation is faster than that of the liquid marbles. The slower evaporation rate of the liquid marble is caused by the additional diffusion barrier imposed by the nanoparticle layer.[4,22,70,72] With surrounding pressure decrease to pressure significantly below the pressure corresponding to the triple point of water, this diffusion barrier prevents significant liquid evaporation from the liquid marble and allows for solidification of the liquid. As shown in Figure 6c, when the pressure is decreased to 300 Pa, the liquid marble shrinks relatively uniformly without the dramatic crumbling and collapse observed in Figure 6a,b.

Breakage of the nanoparticle shell and subsequent emergence of an icicle projecting out of the liquid marble 5 s into the evaporation process clearly demonstrates the freezing of the liquid inside the marble and highlights the almost explosive nature of this forced phase change process (see movie 9 in Supporting Information).

CONCLUSION

In summary, we demonstrate that hydrophobic nanoparticles can self-assemble into elastic films during water condensation and, depending on the wetting properties of the underlying substrate, form flat floating rafts or liquid marbles. The films that form as a result are sufficiently tightly packed to display superhydrophobic characteristics during secondary droplet condensation on their surface. The self-assembly of these films into three-dimensional liquid marbles is driven by multiple coalescence events between partially covered droplets. We also observe that liquid marble formation during water condensation is aided by rapid nanoparticle film redistribution, likely due to the Marangoni effect. Once the droplets become mostly covered, they behave as soft solids and dramatically alter the dynamics of dropwise condensation on the SHS. The process involves a combination of liquid-like and solid-like interactions. As a result, droplet and liquid marble coalescence can occur due to liquid-to-liquid contact or squeezing of the two objects into each other as a result of compressive forces from surrounding droplets and marbles. Irrelevant of the mechanism, coalescence of marbles and drops with diameters above 20 μm causes their rapid movement across the surface. Consequently, the marbles and drops can roll off the edge of the surface and have maximal diameters in the 300 to 400 μm range. Using optical microscopy, we demonstrate that the self-assembled liquid marbles retain their superhydrophobic characteristics over extended periods of time (40 min) under standard conditions for temperature and pressure. We also demonstrate that the randomly moving liquid marbles can be captured and immobilized by site-specific hydrophilic grooves filled with water. Finally, we explore liquid marble and surrounding liquid droplet evaporation due to temperature increase and surrounding pressure decrease. While evaporation behavior during temperature increase or pressure decrease to about 500 Pa did not differ much from previous reports, pressure decrease to 300 Pa caused rapid freezing of the liquid entrapped within the liquid marble highlighted by the dramatic rupture of the nanoparticle layer by icicles generated during the phase change. The condensation-aided liquid marble formation introduced in this work could be extended to the formation of liquid marbles encapsulating a variety of liquids. Furthermore, the introduced method is not sensitive to surrounding conditions and only requires the hydrophobic nanoparticles and the SHS, which can be readily made in a number of economical ways.[37,38,74,75] In contrast, the mixing method requires expensive industrial mixer, and formation of liquid marbles occurs only with a specific water introduction method, mixing rate, and blade orientation.[16,23−25] Thus the condensation-aided liquid marble formation process may be a simple alternative to the industrial mixing method for midscale production of microscale liquid marbles.

METHODS

Wetting Properties of the Utilized Surfaces. We study water condensation occurring on Al_2O_3 nanoparticles dispersed on hydrophilic silicon with a native oxide surface (contact angle of 49 $\pm$ 4°), a hydrophobic silicon surface modified with a perfluorinated silane coating (contact angle of 106 $\pm$ 4°), and a SHS consisting of Al_2O_3 nanoparticles encapsulated in a glass-like matrix and modified with a perfluorinated silane coating (contact angle of 157 $\pm$ 6°). Loose nanoparticles are transferred by dragging a drop of water across the surface, depositing the drop on the unmodified and the modified silicon wafers, and letting the drop evaporate. The about 3 μm thick nanoparticle film and superhydrophobic coating are formed simultaneously during the fabrication process (see details below). The static contact angles were measured using a camera-based system (First 10 Angstroms)[26] with vendor-supplied image capture and analysis software. The reported static contact angles are averages of goniometer measurements in three locations across the surface; the calculated uncertainty is expressed with coverage factor of 2.

Procedure for Perfluorinated Silane Coating of Silicon. Wafers are rinsed with 2-propanol (isopropyl alcohol) and distilled water prior to being placed in a UV ozone cleaner for approximately 15 min for the removal of adventitious hydrocarbon. After cleaning and subsequent rinsing with 2-propanonl, samples are blown dry with nitrogen and placed in a desiccator which is pumped down with house vacuum and brought back to atmospheric pressure with house N_2. Monolayer formation on the wafers by vapor deposition is accomplished by exposure to 1*H*,1*H*,2*H*,2*H*-perfluorodecyltrichlorosilane (Alfa Aesar) in the desiccator under house vacuum for 24−48 h. Wafers are then rinsed with 2-propanol and dried, yielding the hydrophobic silicon surface.

Fabrication Procedure of Al_2O_3 Nanoparticles and Superhydrophobic Surface. The Al_2O_3 nanoparticles as well as the SHS are fabricated using RPX-540 manufactured by Integrated Surface Technologies.[26] The chamber includes inlets for five precursor chemicals and is evacuated using a mechanical pump. An applicator plate, which is located above the substrate to be coated, is permeated with numerous holes to help uniformly disperse the gases over areas as high as several square feet. The Al_2O_3 nanoparticles deposit from the gas phase onto an isopropyl alcohol rinsed silicon wafer. The nanoparticles form in the reaction of trimethylaluminum (TMA) and water vapor: $2Al(CH_3)_3 + 3H_2O \rightarrow Al_2O_3 + 6CH_4$. The reaction takes place in a low-pressure reaction chamber, with injection of TMA at about 27 Pa (200 mTorr) lasting about 3 s followed sequentially by injection of water−alcohol mixture at about 270 Pa (2 Torr) lasting about 20 s. The injection sequence followed by a pump/purge is repeated six times. In order to create the SHS with a multilayer nanoparticle film on top, the interparticle and particle−substrate adhesion is altered by gas phase deposition of thin

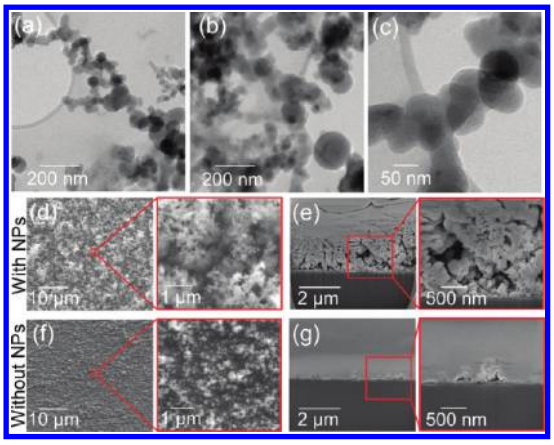

Figure 7. (a−c) TEM images of the hydrophobic nanoparticles dispersed on a holey carbon TEM grid, (d,f) 30° tilt and (e,f) FIB cut 52° cross-sectional SEM images of the of the SHS (d,e) with and (f,g) without loose Al_2O_3 nanoparticles (NPs). The bulk samples were imaged in low-pressure mode with water vapor of 50 Pa, electron beam energy of 5 keV, and spot size 3 to prevent charging, while the cross-sectional samples were locally grounded using a Pt pad and imaged with electron beam energy of 5 keV and current of 0.4 nA in the immersion mode.

SiO_2 encapsulating matrix *via* atomic layer deposition (ALD). The SiO_2 ALD process consists of two self-limiting surface reactions, $SiOH^* + SiCl_4 \rightarrow SiOSiCl_3^* + HCl$ and $SiCl^* + H_2O \rightarrow SiO^* + HCl$, and is catalyzed using pyridine (C_5H_5N).[76,77] About 400 ALD cycles deposited in about 2 h produced about a 40 nm thick SiO_2 layer. In the final fabrication step, the surface with nanoparticles is modified with a functionalization exposure to tridecafluoro-1,1,2,2-tetrahydrooctyltrichlorosilane (FOTS). During fabrication of the superhydrophobic coating, the temperature of the chamber is maintained at 45 °C. After deposition or in the intermediate steps of the deposition process, the residual vapors are pumped/purged out of the chamber with nitrogen gas. The fabrication process produces a 3.16 ± 0.74 μm thick layer of loose nanoparticles with ≈50 to ≈500 nm porosity with underlying ≈150 nm thick surface-bound superhydrophobic film. As shown in TEM images in Figure 7a−c, the nanoparticle layer consists of 10−200 nm diameter particles with irregular shapes. To measure the thickness of the superhydrophobic coating, the loose nanoparticles were removed by acetone rinsing. The top-down as well as cross-sectional images of the SHS with and without the nanoparticle layer are shown in Figure 7d−g. The thickness of the nanoparticle layer is estimated by SEM imaging of the focus ion beam (FIB) cut cross section of the sample (see Supporting Information for details of the FIB cutting process). To characterize the nanoparticle morphology, loose nanoparticle powder was suspended in ethanol, ultrasonicated for 5 min, and drop-casted onto a holey carbon TEM grid, and imaged in TEM (see Supporting Information for imaging conditions). Measurement of the water contact angle with the multilayer nanoparticle film was challenging because even with careful deposition drops tend to bounce and roll off the surface (see Figure 4 in Supporting Information for example). On the basis of the captured images, we estimate the water the contact angle of 160 ± 4° for the surface with nanoparticles. After removal of the multilayer nanoparticle film with acetone rinsing, the surface has a water contact angle of 157 ± 6°.

ESEM Imaging Procedure. Droplet condensation is achieved in the ESEM by increasing the chamber vapor pressure 600 to 900 Pa while the sample temperature is held below the saturation temperature (0 to 7 °C). To prevent condensation during the pump down cycle and prior to imaging, the samples are attached to a stage heated to 15 °C when first introduced into the microscope and are subsequently cooled to −10 to −15 °C at a vapor pressure of 150 Pa for 2 min after two purging cycles. Sustained water condensation is achieved by a step increase in pressure to about 600 Pa followed by a gradual increase to about 900 Pa. Because the water-cooled thermoelectric (Peltier) cooling stage cannot remove all of the heat released by the condensation process, the sample temperature quickly increases to the saturation temperature corresponding to the set chamber vapor pressure. To avoid any electron beam heating effects,[41] the drops are imaged with low electron beam energy of 10 keV and an electron beam current of 0.16 nA. We observe that prolonged direct electron beam exposure of the perfluorinated SHS degrades the surface hydrophobic properties (see Figure 8). The electron-beam-induced wettability change in the surface could be caused by surface damage due to water radiolysis,[78] amorphous carbon film formation,[79,80] or electron-beam-induced dissociation of the surface coating.[81] However, due to the low penetration depth of electrons at 10 keV, once the surface is mostly covered by water, no further degradation of the surface is observed. To prevent electron-beam-induced wettability changes in the surface, the electron beam was blanked prior to initiation of condensation.

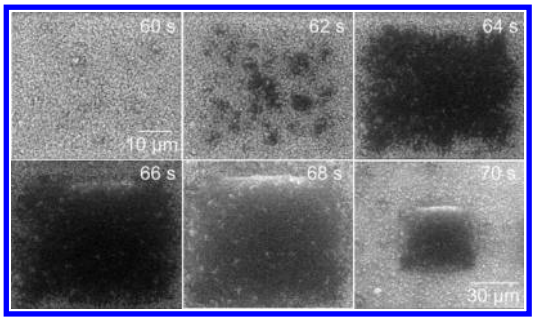

Figure 8. Electron beam damage of the superhydrophobic surface due to prolonged beam exposure.

The dynamics of the condensation process were imaged with 512 pixel × 471 pixel frame sizes and 250 and 750 μs dwell times (0.25 and 0.75 s frame times). The corresponding images were saved every 0.2 s.

Optical Imaging Procedure. The condensation process was also imaged with Leitz Wetzlar Aristomet optical microscope equipped with Jenoptik Progres digital camera with 50 and 100× objectives. The sample was mounted using Antec Formula 5 silver thermal compound to a 1.2 cm × 1.2 cm Analog Technologies thermoelectric cooler module mounted to a 2.5 cm × 5 cm × 5 cm aluminum heat sink. The experiment was performed under standard conditions for temperature and pressure (20 °C and 101.3 kPa) and relative humidity of 40 to 43%, which was continually measured and logged using Lascar EL-USB-2-LCD logger. The thermoelectric cooler module surface temperature was measured using a Fluke thermocouple attached to the surface with the silver thermal compound and electrical tape. Condensation was initiated by quickly decreasing and maintaining the thermoelectric cooler module surface temperature to 0.2 ± 0.2 °C. For each experiment, 694 × 516 pixel images with 100 ms exposure time and 8.5 V illumination were captured with a 5 Hz frequency over 20−40 min. To provide a 10° tilt angle without defocusing part of the viewing area, one side of the microscope was raised about 8 cm (see images of the set up in Supporting Information).

Acknowledgment. This research was performed while K.R. held a National Research Council American Recovery and Reinvestment Act (NRC ARRA) Research Associateship at the National Institute of Standards and Technology in Gaithersburg, MD. Support for this work by Integrated Surface Technologies was provided in part by the National Science Foundation under Grant IIP-1026571. Authors would also like to acknowledge useful discussions with J. Pettibone from NIST.

Supporting Information Available: Movies of all condensation and evaporation processes as well as further information on chamber pressure, total number of drops, and average drop diameter *vs* time, FIB cross-sectioning and imaging procedure, TEM imaging, optical imaging setup,

and contact angle measurement on superhydrophobic surface with the nanoparticle film. This material is available free of charge *via* the Internet at http://pubs.acs.org.

REFERENCES AND NOTES

1. Vella, D.; Mahadevan, L. The Cheerios Effect. *Am. J. Phys.* **2005**, *73*, 817–825.
2. Larmour, I. A.; Saunders, G. C.; Bell, S. E. J. Sheets of Large Superhydrophobic Metal Particles Self Assembled on Water by the Cheerios Effect. *Angew. Chem., Int. Ed.* **2008**, *47*, 5043–5045.
3. Vella, D.; Aussillous, P.; Mahadevan, L. Elasticity of an Interfacial Particle Raft. *Europhys. Lett.* **2004**, *68*, 212–218.
4. Bhosale, P. S.; Panchagnula, M. V.; Stretz, H. A. Mechanically Robust Nanoparticle Stabilized Transparent Liquid Marbles. *App. Phys. Lett.* **2008**, *93*, 034109-1–034109-3.
5. Aussillous, P.; Quere, D. Liquid Marbles. *Nature* **2001**, *411*, 924–927.
6. Bormashenko, E.; Bormashenko, Y.; Musin, A. Water Rolling and Floating upon Water: Marbles Supported by a Water/Marble Interface. *J. Colloid Interface Sci.* **2009**, *333*, 419–421.
7. McHale, G.; Newton, M. I. Liquid Marbles: Principles and Applications. *Soft Matter* **2011**, *7*, 5473–5481.
8. Bormashenko, E. Liquid Marbles: Properties and Applications. *Curr. Opin. Colloid Interface Sci.* **2010**, *16*, 266–271.
9. Aussillous, P.; Qu; Eacute; David Shapes of Rolling Liquid Drops. *J. Fluid Mech.* **2004**, *512*, 133–151.
10. Aussillous, P.; Quere, D. Properties of Liquid Marbles. *Philos. Trans. R. Soc. A* **2006**, *462*, 973–999.
11. McHale, G.; Shirtcliffe, N. J.; Newton, M. I.; Pyatt, F. B.; Doerr, S. H. Self-Organization of Hydrophobic Soil and Granular Surfaces. *App. Phys. Lett.* **2007**, *90*, 054110-1–054110-3.
12. Pike, N.; Richard, D.; Foster, W.; Mahadevan, L. How Aphids Lose Their Marbles. *Philos. Trans. R. Soc. B* **2002**, *269*, 1211–1215.
13. Weiss, M. R. Defecation Behavior and Ecology of Insects. *Annu. Rev. Entomol.* **2006**, *51*, 635–661.
14. Eshtiaghi, N.; Hapgood, K. P. A Quantitative Framework for the Formation of Liquid Marbles and Hollow Granules from Hydrophobic Powders. *Powder Technol.* **2011**, DOI: 10.1016/j.powtec.2011.05.007.
15. Gao, L.; McCarthy, T. J. Ionic Liquid Marbles. *Langmuir* **2007**, *23*, 10445–10447.
16. Forny, L.; Pezron, I.; Saleh, K.; Guigon, P.; Komunjer, L. Storing Water in Powder Form by Self-Assembling Hydrophobic Silica Nanoparticles. *Powder Technol.* **2007**, *171*, 15–24.
17. Xue, Y.; Wang, H.; Zhao, Y.; Dai, L.; Feng, L.; Wang, X.; Lin, T. Magnetic Liquid Marbles: A "Precise" Miniature Reactor. *Adv. Mater.* **2010**, *22*, 4814–4818.
18. Tian, J.; Arbatan, T.; Li, X.; Shen, W. Liquid Marble for Gas Sensing. *Chem. Commun.* **2010**, *46*, 4734–4736.
19. Tian, J.; Arbatan, T.; Li, X.; Shen, W. Porous Liquid Marble Shell Offers Possibilities for Gas Detection and Gas Reactions. *Chem. Eng. J.* **2010**, *165*, 347–353.
20. Bormashenko, E.; Musin, A. Revealing of Water Surface Pollution with Liquid Marbles. *Appl. Surf. Sci.* **2009**, *255*, 6429–6431.
21. Bormashenko, E.; Balter, R.; Aurbach, D. Micropump Based on Liquid Marbles. *Appl. Phys. Lett.* **2010**, *97*, 091908-1–091908-2.
22. Bhosale, P. S.; Panchagnula, M. V. On Synthesizing Solid Polyelectrolyte Microspheres from Evaporating Liquid Marbles. *Langmuir* **2010**, *26*, 10745–10749.
23. Forny, L.; Saleh, K.; Pezron, I.; Komunjer, L.; Guigon, P. Influence of Mixing Characteristics for Water Encapsulation by Self-Assembling Hydrophobic Silica Nanoparticles. *Powder Technol.* **2009**, *189*, 263–269.
24. Forny, L.; Saleh, K.; Denoyel, R.; Pezron, I. Contact Angle Assessment of Hydrophobic Silica Nanoparticles Related to the Mechanisms of Dry Water Formation. *Langmuir* **2009**, *26*, 2333–2338.
25. Saleh, K.; Forny, L.; Guigon, P.; Pezron, I. Dry Water: From Physico-Chemical Aspects to Process-Related Parameters. *Chem. Eng. Res. Des.* **2011**, *89*, 537–544.
26. Certain commercial equipment, instruments, and materials are identified in this Publication to adequately specify the experimental procedure. Such identification in no way implies approval, recommendation, or endorsement by NIST, nor does it imply that the equipment, instruments, or materials edentified are necessarily the best available for the purpose.
27. Chinn, J.; Helmrich, F.; Guenther, R.; Wiltse, M.; Hurst, K.; Ashurst, R. W. Durable Super-Hydrophobic Nano-Composite Films. In *NSTI-Nanotech 2010*, 2010; Vol. 1.
28. Mockenhaupt, B.; Ensikat, H.-J.; Spaeth, M.; Barthlott, W. Superhydrophobicity of Biological and Technical Surfaces under Moisture Condensation: Stability in Relation to Surface Structure. *Langmuir* **2008**, *24*, 13591–13597.
29. Zheng, Y. M.; Han, D.; Zhai, J.; Jiang, L. *In Situ* Investigation on Dynamic Suspending of Microdroplet on Lotus Leaf and Gradient of Wettable Micro- and Nanostructure from Water Condensation. *Appl. Phys. Lett.* **2008**, *92*, 084106-1–084106-3.
30. Boreyko, J. B.; Chen, C. H. Restoring Superhydrophobicity of Lotus Leaves with Vibration-Induced Dewetting. *Phys. Rev. Lett.* **2009**, *103*, 174502-1–174502-4.
31. Boreyko, J. B.; Chen, C. H. Self-Propelled Dropwise Condensate on Superhydrophobic Surfaces. *Phys. Rev. Lett.* **2009**, *103*, 184501-1–184501-4.
32. Chen, C. H.; Cai, Q. J.; Tsai, C. L.; Chen, C. L.; Xiong, G. Y.; Yu, Y.; Ren, Z. F. Dropwise Condensation on Superhydrophobic Surfaces with Two-Tier Roughness. *Appl. Phys. Lett.* **2007**, *90*, 173108-1–173108-3.
33. Dorrer, C.; Ruhe, J. Wetting of Silicon Nanograss: From Superhydrophilic to Superhydrophobic Surfaces. *Adv. Mater.* **2008**, *20*, 159–163.
34. Lau, K. K. S.; Bico, J.; Teo, K. B. K.; Chhowalla, M.; Amaratunga, G. A. J.; Milne, W. I.; McKinley, G. H.; Gleason, K. K. Superhydrophobic Carbon Nanotube Forests. *Nano Lett.* **2003**, *3*, 1701–1705.
35. Dietz, C.; Rykaczewski, K.; Fedorov, A. G.; Joshi, Y. Visualization of Droplet Departure on a Superhydrophobic Surface and Implications to Heat Transfer Enhancement During Dropwise Condensation. *Appl. Phys. Lett.* **2010**, *97*, 033104-1–033104-4.
36. Ke, Q.; Zhang, S.; Tang, T.; Wang, S.; Jing, H. Intrinsic Dew-Enhancing Ability of SiO_2/Pods Materials. *Colloids Surf. A* **2011**, *377*, 110–114.
37. Feng, L.; Li, S.; Li, Y.; Li, H.; Zhang, L.; Zhai, J.; Song, Y.; Liu, B.; Jiang, L.; Zhu, D. Super-Hydrophobic Surfaces: From Natural to Artificial. *Adv. Mater.* **2002**, *14*, 1857–1860.
38. Sun, T.; Feng, L.; Gao, X.; Jiang, L. Bioinspired Surfaces with Special Wettability. *Acc. Chem. Res.* **2005**, *38*, 644–652.
39. Rykaczewski, K.; Scott, J. H. J.; Rajauria, S.; Chinn, J.; Chinn, A. M.; Jones, W. Three Dimensional Aspects of Droplet Coalescence During Dropwise Condensation on Superhydrophobic Surfaces. *Soft Matter* **2011**, *7*, 8749–8752.
40. Rykaczewski, K.; Scott, J. H. J. Methodology for Imaging Nano-to-Microscale Water Condensation Dynamics on Complex Nanostructures. *ACS Nano* **2011**, *5*, 5926–5968.
41. Rykaczewski, K.; Scott, J. H. J.; Fedorov, A. G. Electron Beam Heating Effects during Environmental Scanning Electron Microscopy Imaging of Water Condensation on Superhydrophobic Surfaces. *Appl. Phys. Lett.* **2011**, *98*, 093106-1–093106-3.
42. Shirtcliffe, N. J.; McHale, G.; Newton, M. I.; Pyatt, B. F.; Doerr, S. H. Critical Conditions for the Wetting of Soils. *Appl. Phys. Lett.* **2006**, *89*, 094101-1–094101-3.
43. McHale, G.; Shirtcliffe, N. J.; Newton, M. I.; Pyatt, F. B. Implications of Ideas on Super-Hydrophobicity for Water Repellent Soil. *Hydrol. Processes* **2007**, *21*, 2229–2238.
44. Gemici, Z.; Schwachulla, P. I.; Williamson, E. H.; Rubner, M. F.; Cohen, R. E. Targeted Functionalization of Nanoparticle Thin Films *via* Capillary Condensation. *Nano Lett.* **2009**, *9*, 1064–1070.
45. Beysens, D.; Knobler, C. M. Growth of Breath Figures. *Phys. Rev. Lett.* **1986**, *57*, 1433–1436.
46. Viovy, J. L.; Beysens, D.; Knobler, C. M. Scaling Description for the Growth of Condensation Patterns on Surfaces. *Phys. Rev. A* **1988**, *37*, 4965–4970.

47. Beysens, D.; Knobler, C. M.; Schaffar, H. Scaling in the Growth of Aggregates on a Surface. *Phys. Rev. B* **1990**, *41*, 9814–9818.
48. Beysens, D. Dew Nucleation and Growth. *C. R. Phys.* **2006**, *7*, 1082–1100.
49. Narhe, R. D.; Beysens, D. A. Nucleation and Growth on a Superhydrophobic Grooved Surface. *Phys. Rev. Lett.* **2004**, *93*, 076103.
50. Narhe, R. D.; Beysens, D. A. Water Condensation on a Super-Hydrophobic Spike Surface. *Europhys. Lett.* **2006**, *75*, 98–104.
51. Narhe, R. D.; Beysens, D. A. Growth Dynamics of Water Drops on a Square-Pattern Rough Hydrophobic Surface. *Langmuir* **2007**, *23*, 6486–6489.
52. Narhe, R. D.; González-Viñas, W.; Beysens, D. A. Water Condensation on Zinc Surfaces Treated by Chemical Bath Deposition. *Appl. Surf. Sci.* **2011**, *256*, 4930–4933.
53. Chen, X.; Wu, J.; Ma, R.; Hua, M.; Koratkar, N.; Yao, S.; Wang, Z. Nanograssed Micropyramidal Architectures for Continuous Dropwise Condensation. *Adv. Funct. Mater.* **2011**, DOI: 10.1002/adfm.201101302.
54. Anand, S.; Son, S. Y. Sub-micrometer Dropwise Condensation under Superheated and Rarefied Vapor Condition. *Langmuir* **2010**, *26*, 17100–17110.
55. Bormashenko, E.; Bormashenko, Y. Non-stick Droplet Surgery with a Superhydrophobic Scalpel. *Langmuir* **2010**, *27*, 3266–3270.
56. Eshtiaghi, N.; Liu, J. S.; Shen, W.; Hapgood, K. P. Liquid Marble Formation: Spreading Coefficients or Kinetic Energy? *Powder Technol.* **2009**, *196*, 126–132.
57. Hapgood, K. P.; Farber, L.; Michaels, J. N. Agglomeration of Hydrophobic Powders *via* Solid Spreading Nucleation. *Powder Technol.* **2009**, *188*, 248–254.
58. Hapgood, K. P.; Khanmohammadi, B. Granulation of Hydrophobic Powders. *Powder Technol.* **2009**, *189*, 253–262.
59. Nguyen, T. H.; Eshtiaghi, N.; Hapgood, K. P.; Shen, W. An Analysis of the Thermodynamic Conditions for Solid Powder Particles Spreading over Liquid Surface. *Powder Technol.* **2010**, *201*, 306–310.
60. McEleney, P.; Walker, G. M.; Larmour, I. A.; Bell, S. E. J. Liquid Marble Formation Using Hydrophobic Powders. *Chem. Eng. J.* **2009**, *147*, 373–382.
61. Aarts, D. G. A. L.; Lekkerkerker, H. N. W.; Guo, H.; Wegdam, G. H.; Bonn, D. Hydrodynamics of Droplet Coalescence. *Phys. Rev. Lett.* **2005**, *95*, 164503-1–164503-4.
62. Tam, D.; von Arnim, V.; McKinley, G. H.; Hosoi, A. E. Marangoni Convection in Droplets on Superhydrophobic Surfaces. *J. Fluid Mech.* **2009**, *624*, 101–123.
63. Dorvee, J. R.; Derfus, A. M.; Bhatia, S. N.; Sailor, M. J. Manipulation of Liquid Droplets Using Amphiphilic, Magnetic One-Dimensional Photonic Crystal Chaperones. *Nat. Mater.* **2004**, *3*, 896–899.
64. Bormashenko, E.; Bormashenko, Y.; Pogreb, R.; Gendelman, O. Janus Droplets: Liquid Marbles Coated with Dielectric/Semiconductor Particles. *Langmuir* **2011**, *27*, 7–10.
65. Zhao, Y.; Fang, J.; Wang, H.; Wang, X.; Lin, T. Magnetic Liquid Marbles: Manipulation of Liquid Droplets Using Highly Hydrophobic Fe_3O_4 Nanoparticles. *Adv. Mater.* **2009**, *22*, 707–710.
66. Bormashenko, E.; Pogreb, R.; Bormashenko, Y.; Musin, A.; Stein, T. New Investigations on Ferrofluidics: Ferrofluidic Marbles and Magnetic-Field-Driven Drops on Superhydrophobic Surfaces. *Langmuir* **2008**, *24*, 12119–12122.
67. Wang, F.-C.; Yang, F.; Zhao, Y.-P. Size Effect on the Coalescence-Induced Self-Propelled Droplet. *Appl. Phys. Lett.* **2011**, *98*, 053112-1–053112-4.
68. Varanasi, K. K.; Hsu, M.; Bhate, N.; Yang, W.; Deng, T. Spatial Control in the Heterogeneous Nucleation of Water. *Appl. Phys. Lett.* **2009**, *95*, 094101.
69. Zeng, C.; Bissig, H.; Dinsmore, A. D. Particles on Droplets: From Fundamental Physics to Novel Materials. *Solid State Commun.* **2006**, *139*, 547–556.
70. Dandan, M.; Erbil, H. Y. Evaporation Rate of Graphite Liquid Marbles: Comparison with Water Droplets. *Langmuir* **2009**, *25*, 8362–8367.
71. Fujii, S.; Kameyama, S.; Armes, S. P.; Dupin, D.; Suzaki, M.; Nakamura, Y. pH-Responsive Liquid Marbles Stabilized with Poly(2-vinylpyridine) Particles. *Soft Matter* **2011**, *6*, 635–640.
72. Tosun, A.; Erbil, H. Y. Evaporation Rate of PtFe Liquid Marbles. *Appl. Surf. Sci.* **2009**, *256*, 1278–1283.
73. Smith, R. G. Wax Glands, Wax Production and the Functional Significance of Wax Use in Three Aphid Species (Homoptera: Aphididae). *J. Nat. Hist.* **1999**, *33*, 513–530.
74. Li, X.-M.; Reinhoudt, D.; Crego-Calama, M. What Do We Need for a Superhydrophobic Surface? A Review on the Recent Progress in the Preparation of Superhydrophobic Surfaces. *Chem. Soc. Rev.* **2007**, *36*, 1350–1368.
75. Roach, P.; Shirtcliffe, N. J.; Newton, M. I. Progess in Superhydrophobic Surface Development. *Soft Matter* **2008**, *4*, 224–240.
76. Klaus, J. W.; George, S. M. Atomic Layer Deposition of SiO_2 at Room Temperature Using NH_3-Catalyzed Sequential Surface Reactions. *Surf. Sci.* **2000**, *447*, 81–90.
77. Du, Y.; Du, X.; George, S. M. SiO_2 Film Growth at Low Temperatures by Catalyzed Atomic Layer Deposition in a Viscous Flow Reactor. *Thin Solid Films* **2005**, *491*, 43–53.
78. Royall, C. P.; Thiel, B. L.; Donald, A. M. Radiation Damage of Water in Environmental Scanning Electron Microscopy. *J. Microsc.* **2001**, *204*, 185–195.
79. Aronov, D.; Molotskii, M.; Rosenman, G. Electron-Induced Wettability Modification. *Phys. Rev. B* **2007**, *76*, 035437-1–035437-12.
80. Aronov, D.; Rosenman, G.; Barkay, Z. Wettability Study of Modified Silicon Dioxide Surface Using Environmental Scanning Electron Microscopy. *J. Appl. Phys.* **2007**, *101*, 084901-1–084901-5.
81. Bozso, F.; Avouris, P. Thermal and Electron-Beam-Induced Reaction of Disilane on Si(100). *Phys. Rev. B* **1988**, *38*, 3943–3947.